Global Journal of Pure and Applied Mathematics.
ISSN 0973-1768 Volume 22, Number 2 (2026), pp. 445–469

https://www.ripublication.com

Nonuniform-Grid IMEX and Crank–Nicolson Schemes for Boundary Quenching in a Christov–Deng Type Problem

Thibaut K. KOUAKOU[1] **and Nabongo DIABATE**[2]

[1]*Université Nangui Abrogoua, UFR des Sciences Fondamentales et Appliquées (UFR-SFA), Laboratoire de Mathématiques et Informatique, 02 BP 801 Abidjan 02, Côte d'Ivoire. Email: kkthibaut@yahoo.fr. ORCID: 0009-0003-6792-251X.*
[2]*Université Alassane Ouattara, UFR des Sciences et Technologie (UFR-ST), BP V 18 Bouaké 01, Côte d'Ivoire. Email: nabongo_diabate@yahoo.fr. ORCID: 0009-0004-4420-3034.*

Abstract

We analyze IMEX and Crank–Nicolson finite-difference approximations on nonuniform grids for a nonlinear diffusion equation with a singular Neumann boundary condition. The solution remains positive before quenching and reaches the singular level at the active boundary in finite time. The spatial grid is fixed and refined near that boundary. We construct conservative nonuniform finite-difference operators and adaptive time discretizations that keep the boundary value positive before the numerical hitting time. Positivity follows from inverse positivity of tridiagonal M-matrices. Subcritical stability is proved under a discrete diffusion bound, and a weighted balance yields finite-time numerical hitting; for $\gamma = 1$ the balance is an exact identity. We prove convergence before quenching and convergence of subcritical hitting times. Numerical tests compare the two schemes, quantify the effect of mesh concentration, and verify the boundary rate predicted by the continuous theory.

2020 Mathematics Subject Classification. 35K65, 35B44, 65M06, 65M12, 65M20.

Key words and phrases. Boundary quenching; nonlinear diffusion; singular Neumann condition; nonuniform grid; IMEX scheme; Crank–Nicolson scheme; adaptive time step; numerical quenching time.

1. INTRODUCTION

We consider the nonlinear diffusion problem

$$\begin{cases} u^{\gamma-1}u_t = u_{xx}, & 0 < x < 1, \quad 0 < t < T, \\ u_x(0,t) = u(0,t)^{-\beta}, & 0 < t < T, \\ u_x(1,t) = 0, & 0 < t < T, \\ u(x,0) = u_0(x), & 0 \le x \le 1, \end{cases} \tag{1}$$

where

$$\beta > 0, \qquad \gamma > 0. \tag{2}$$

The solution is positive as long as it is classical. Boundary quenching means that

$$\lim_{t \to T_q^-} u(0,t) = 0,$$

while the solution remains positive on each compact subinterval of $[0, T_q)$. The singularity is created by the boundary flux, not by an interior reaction term. When $u(0,t)$ becomes small, the imposed derivative $u(0,t)^{-\beta}$ becomes large and drives the boundary value toward the singular level.

Boundary quenching problems of this type are mathematical models for finite-time loss of regularity caused by a boundary transfer law. They appear as reduced descriptions of heat conduction with nonlinear boundary feedback, diffusion with boundary-controlled reactions, and quenching analogues in which the singularity is generated at the boundary rather than by an interior source. The active boundary is therefore the part of the domain where the numerical grid must resolve the largest gradients.

The numerical motivation begins with the work of Christov and Deng [3]. They approximated (1) by a finite-difference method adapted to the energy balance and used a nonuniform mesh refined near $x = 0$, the quenching boundary. For this boundary singularity, such a grid places more nodes in the region where the gradient varies most. A uniform grid instead allocates many points to regions where the solution is smooth and too few points near the active boundary. General discussions of nonuniform finite differences and their effect on truncation errors may be found in Jones and Thompson [11], Veldman and Rinzema [23], Samarskii [22], and later analyses of central differences on nonuniform grids [2, 24].

The present paper keeps this boundary refinement and studies the time discretization on the same grid. We compare an IMEX scheme with a Crank–Nicolson diffusion average. The singular boundary flux is treated explicitly at the known time level, and

the time step is restricted so that the discrete boundary value remains positive before the numerical hitting time. The diffusion part is implicit in the IMEX method and trapezoidal in the Crank–Nicolson method. This separation gives a direct comparison between a positivity-preserving M-matrix step and a diffusion average with an additional positivity check.

The analysis of quenching with nonlinear boundary conditions has been developed in [1, 6, 7, 12, 15, 16]. The singular behavior of the time derivative near quenching and the boundary rate for the nonlinear diffusion model considered here are discussed in [4, 5]. The local existence and uniqueness framework used below is the classical parabolic one: on every interval where the solution is bounded away from the singular level, the equation is uniformly parabolic and the nonlinear boundary map is smooth. We use the standard continuation and comparison principles from Friedman [8], Ladyzhenskaya, Solonnikov and Ural'tseva [13], Lieberman [19], Pao [20], and Protter and Weinberger [21]. These continuous estimates provide the reference rate used to test the nonuniform-grid IMEX and Crank–Nicolson discretizations. The adaptive time stepping used below is related to mesh-dependent time steps and moving-mesh methods for singular parabolic equations [18, 17].

A second point concerns estimates compatible with the regularity of the data. For generalized solutions and nonuniform grids, Taylor expansion alone can impose unnecessary smoothness assumptions. Lazarov, Makarov and Samarskii [14], Jovanović and Matus [9], and Jovanović [10] developed convergence estimates in discrete Sobolev norms and used averaged right-hand sides on nonuniform meshes. We follow this principle in a subcritical setting: the convergence theorem is first stated with the actual discrete consistency defect. A second-order spatial estimate is then obtained only when the boundary row has the corresponding consistency.

The main results are the following. First, the IMEX scheme and the Crank–Nicolson diffusion-average scheme are shown to preserve positivity through inverse-positive tridiagonal M-matrices under explicit time-step restrictions. Second, a weighted discrete balance gives a finite-time threshold-hitting estimate; for $\gamma = 1$ this balance is an exact identity. Third, a subcritical stability theorem and a consistency argument yield convergence before quenching and convergence of regular threshold hitting times. Fourth, the numerical tests show stabilization of the hitting time, improvement due to boundary mesh concentration, and agreement with the boundary rate of Deng and Xu.

The paper is organized as follows. Section 2 recalls the continuous boundary-quenching problem. Section 3 introduces the nonuniform mesh and the finite-difference operators. Sections 4 and 5 define the IMEX and Crank–Nicolson schemes. Section 6 proves

positivity, comparison and subcritical stability. Section 7 studies finite-time numerical hitting and localization. Section 8 proves convergence before quenching and convergence of subcritical hitting times. Section 9 gives numerical tests.

2. CONTINUOUS BOUNDARY-QUENCHING PROBLEM

We first recall the continuous properties that the schemes must preserve. The local theory is invoked only on subcritical strips. If $u \geq \eta > 0$, then the coefficient $u^{1-\gamma}$ and the boundary map $u \mapsto u^{-\beta}$ are smooth and locally Lipschitz. Classical parabolic theory for nonlinear boundary conditions then gives local existence, uniqueness, and continuation as long as the positive lower bound is preserved; see [8, 13, 19, 20]. The next proposition records the precise form needed later in the numerical analysis. We assume

$$u_0 \in C^2([0,1]), \qquad u_0(x) > 0, \tag{3}$$

with the compatibility and monotonicity conditions

$$u_0'(0) = u_0(0)^{-\beta}, \qquad u_0'(1) = 0, \qquad u_0'(x) \geq 0 \quad (0 \leq x \leq 1). \tag{4}$$

These assumptions keep the comparison argument transparent. They are not intended to be optimal.

Proposition 2.1. *Assume* (2)*,* (3) *and* (4)*. Then problem* (1) *has a maximal positive classical solution*

$$u \in C^{2,1}((0,1) \times (0, T_{\max})) \cap C([0,1] \times [0, T_{\max})).$$

For each $T < T_{\max}$, there exists $\eta_T > 0$ such that

$$u(x,t) \geq \eta_T, \qquad 0 \leq x \leq 1, \qquad 0 \leq t \leq T.$$

If $T_{\max} < \infty$, then

$$\lim_{t \to T_{\max}^-} \min_{0 \leq x \leq 1} u(x,t) = 0.$$

Proof. Choose $\eta > 0$ such that $u_0 \geq 2\eta$ on $[0,1]$. In the region $v \geq \eta$, the coefficient $v^{1-\gamma}$ in the equation $u_t = u^{1-\gamma} u_{xx}$ and the boundary nonlinearity $v^{-\beta}$ are smooth and locally Lipschitz. The problem is therefore a uniformly parabolic equation with a smooth nonlinear Neumann boundary condition on this subcritical set. The classical results on quasilinear parabolic equations and nonlinear boundary conditions give a unique local classical solution; see, for example, [8, 13, 19, 20]. The compatibility conditions in (4) ensure that the boundary conditions hold at $t = 0$.

The parabolic minimum principle gives positivity as long as the solution remains classical. An interior first contact with the level zero is impossible on any interval where the solution is bounded below by a positive constant. At the right boundary, the homogeneous Neumann condition prevents the creation of a negative boundary minimum. At the active boundary, the prescribed flux is singular at zero and a classical positive solution cannot cross the singular level.

For $T < T_{\max}$, compactness of $[0,1] \times [0,T]$ gives a positive lower bound η_T. If a finite maximal time were reached while the solution remained uniformly separated from zero, all coefficients in the equation and in the boundary condition would remain locally Lipschitz. The continuation theorem would then extend the solution beyond $T_{\max}$, which contradicts maximality. Hence finite maximal time can occur only by loss of positivity. □

The monotonicity of the initial datum identifies the active boundary.

Lemma 2.1. *Under the hypotheses of Proposition 2.1, the maximal solution satisfies*

$$u_x(x,t) \geq 0, \qquad 0 \leq x \leq 1, \qquad 0 < t < T_{\max}.$$

Consequently,

$$\min_{0 \leq x \leq 1} u(x,t) = u(0,t), \qquad 0 < t < T_{\max}.$$

Proof. Let $T < T_{\max}$. By Proposition 2.1, $u \geq \eta_T > 0$ on $[0,1] \times [0,T]$. Set $w = u_x$. Differentiating $u_t = u^{1-\gamma} u_{xx}$ with respect to x gives

$$w_t - u^{1-\gamma} w_{xx} - (1-\gamma) u^{-\gamma} u_{xx} w = 0.$$

The coefficients are bounded on $[0,1] \times [0,T]$, and $u^{1-\gamma}$ is bounded away from zero and infinity there. The initial condition gives $w(x,0) = u_0'(x) \geq 0$. The boundary values are

$$w(0,t) = u(0,t)^{-\beta} > 0, \qquad w(1,t) = 0.$$

The maximum principle applied to this linear equation yields $w \geq 0$ on $[0,1] \times [0,T]$. Since $T < T_{\max}$ is arbitrary, the result follows. The identity for the minimum is immediate. □

Theorem 2.1. *Assume* (2)*,* (3) *and* (4)*. Then the maximal time is finite and the solution quenches at the left boundary:*

$$T_q = T_{\max} < \infty, \qquad \lim_{t \to T_q^-} u(0,t) = 0.$$

Moreover, if

$$E(t) = \int_0^1 u(x,t)^\gamma \, \mathrm{d}x,$$

then

$$T_q \leq \frac{E(0)^{1+\beta/\gamma}}{\gamma+\beta}. \tag{5}$$

Proof. Multiplying the equation by γ and integrating over $(0,1)$, we obtain

$$E'(t) = \gamma \int_0^1 u_{xx}(x,t)\, \mathrm{d}x = \gamma\big(u_x(1,t) - u_x(0,t)\big) = -\gamma u(0,t)^{-\beta}.$$

By Lemma 2.1, $u(0,t) \leq u(x,t)$ on $[0,1]$. Hence

$$u(0,t)^\gamma \leq E(t), \qquad u(0,t)^{-\beta} \geq E(t)^{-\beta/\gamma}.$$

It follows that

$$E'(t) \leq -\gamma E(t)^{-\beta/\gamma}.$$

As long as $E(t) > 0$,

$$\frac{\mathrm{d}}{\mathrm{d}t} E(t)^{1+\beta/\gamma} = \left(1 + \frac{\beta}{\gamma}\right) E(t)^{\beta/\gamma} E'(t) \leq -(\gamma+\beta).$$

After integration from 0 to t, $E(t)$ cannot stay positive beyond the time in (5). Thus $T_{\max} < \infty$. Proposition 2.1 and Lemma 2.1 show that the vanishing point is $x = 0$. □

The boundary rate is used only as a numerical diagnostic.

Proposition 2.2. *Under the hypotheses of the boundary-quenching theory of Deng and Xu [5], there are constants $c_1, c_2 > 0$ such that, for t sufficiently close to T_q,*

$$c_1(T_q - t)^{1/(\gamma+2\beta+1)} \leq u(0,t) \leq c_2(T_q - t)^{1/(\gamma+2\beta+1)}. \tag{6}$$

Proof. This is the boundary quenching-rate estimate established for this singular Neumann problem in Deng and Xu [5]; see also the numerical investigation of Christov and Deng [3]. The exponent is consistent with the formal boundary-layer scale $-m'(t) \asymp m(t)^{-\gamma-2\beta}$ for $m(t) = u(0,t)$. □

3. NONUNIFORM MESH AND FINITE-DIFFERENCE OPERATORS

Let $I \geq 2$ and let

$$0 = x_0 < x_1 < \cdots < x_I = 1$$

be a fixed nonuniform grid. Put

$$h_i = x_i - x_{i-1}, \qquad 1 \leq i \leq I, \qquad h_{\min} = \min_{1 \leq i \leq I} h_i, \qquad H = \max_{1 \leq i \leq I} h_i.$$

The grid is refined near $x = 0$. The discrete maximum-norm arguments below use only positivity of the mesh widths. Consistency estimates on a sequence of grids use the local smoothness condition stated after the stretching formula. In the numerical tests we use the smooth stretching

$$x_i = \frac{\exp(\alpha i/I) - 1}{\exp(\alpha) - 1}, \qquad 0 \leq i \leq I, \qquad \alpha > 0. \tag{7}$$

The parameter α controls the concentration near the active boundary. Large values of α may produce an excessively small h_1 and increase the stiffness of the discrete problem.

Assumption 3.1. *When a second-order consistency estimate is invoked, the family of grids satisfies*

$$H \to 0, \qquad H^* := \max_{1 \leq i \leq I-1} |h_{i+1} - h_i| \leq C_m H^2,$$

with a constant C_m independent of I. The exponential grid (7) *satisfies this condition when α is fixed. The positivity and M-matrix results do not require this assumption.*

For a grid vector $V = (V_0, \ldots, V_I)^T \in \mathbb{R}^{I+1}$, define

$$D_h^+ V_0 = \frac{V_1 - V_0}{h_1}, \qquad D_h^- V_I = \frac{V_I - V_{I-1}}{h_I}.$$

For $1 \leq i \leq I - 1$, set

$$\delta_h^2 V_i = \frac{2}{h_i + h_{i+1}} \left(\frac{V_{i+1} - V_i}{h_{i+1}} - \frac{V_i - V_{i-1}}{h_i} \right).$$

The boundary rows are defined from the same finite-volume balance as in Christov and Deng's semidiscrete approximation:

$$(A_h V)_0 = \frac{2}{h_1} D_h^+ V_0, \qquad (A_h V)_I = -\frac{2}{h_I} D_h^- V_I,$$

while

$$(A_h V)_i = \delta_h^2 V_i, \qquad 1 \leq i \leq I - 1.$$

Thus A_h is tridiagonal with negative diagonal entries and nonnegative off-diagonal entries. It is the discrete diffusion operator associated with the Neumann conditions when the singular boundary flux is moved to the right-hand side.

We use the finite-volume weights

$$\omega_0 = \frac{h_1}{2}, \qquad \omega_i = \frac{h_i + h_{i+1}}{2} \quad (1 \le i \le I-1), \qquad \omega_I = \frac{h_I}{2}.$$

They satisfy the discrete Green identity

$$\sum_{i=0}^{I} \omega_i (A_h V)_i = 0, \qquad V \in \mathbb{R}^{I+1}. \tag{8}$$

Indeed, after multiplication by the weights, the nearest-neighbor fluxes telescope and the boundary contributions cancel. If

$$S_0(V) = -\frac{2}{h_1} V_0^{-\beta}, \qquad S_i(V) = 0 \quad (1 \le i \le I),$$

then

$$\sum_{i=0}^{I} \omega_i \big((A_h V)_i + S_i(V) \big) = -V_0^{-\beta}. \tag{9}$$

This is the discrete counterpart of the continuous energy balance.

The discrete cone used below is

$$K_h = \{ V \in \mathbb{R}^{I+1} : 0 < V_0 \le V_1 \le \cdots \le V_I \}.$$

For vectors in K_h, the discrete minimum is the active boundary value V_0.

The semidiscrete problem associated with (1) is

$$\begin{cases} U_0(t)^{\gamma-1} \dfrac{\mathrm{d}U_0}{\mathrm{d}t}(t) = (A_h U(t))_0 - \dfrac{2}{h_1} U_0(t)^{-\beta}, \\ U_i(t)^{\gamma-1} \dfrac{\mathrm{d}U_i}{\mathrm{d}t}(t) = (A_h U(t))_i, \qquad 1 \le i \le I, \\ U_i(0) = u_0(x_i), \qquad 0 \le i \le I. \end{cases}$$

The negative boundary source decreases the active boundary value and produces numerical quenching.

Lemma 3.1. *Let $C = \mathrm{diag}(c_0, \ldots, c_I)$ with $c_i > 0$. For every $\sigma > 0$ and every $\Delta t > 0$, the matrix*

$$M_\sigma = C - \sigma \Delta t A_h$$

is a nonsingular M-matrix. Consequently, $M_\sigma^{-1} \ge 0$ componentwise.

Proof. The off-diagonal entries of $-A_h$ are nonpositive, while the diagonal entries of $-A_h$ are nonnegative. Thus M_σ is a Z-matrix. We verify strict diagonal dominance. For the left boundary row,

$$c_0 + \sigma\Delta t\frac{2}{h_1^2} > \sigma\Delta t\frac{2}{h_1^2}.$$

For $1 \le i \le I-1$, the diagonal entry is

$$c_i + \sigma\Delta t\frac{2}{h_i + h_{i+1}}\left(\frac{1}{h_i} + \frac{1}{h_{i+1}}\right),$$

whereas the sum of the absolute values of the two off-diagonal entries is the same expression without c_i. The right boundary row is identical in structure to the left one. Hence each row is strictly diagonally dominant with a positive diagonal. A strictly diagonally dominant Z-matrix with positive diagonal entries is a nonsingular M-matrix. Since the tridiagonal graph is connected, the matrix is irreducible, and its inverse is componentwise nonnegative; in fact it is strictly positive. □

4. THE IMEX SCHEME

We now define the first time discretization. The diffusion is implicit, while the singular boundary flux is evaluated at the previous time level.

Let $0 = t_0 < t_1 < \cdots$ be a variable time grid, with $\Delta t_n = t_{n+1} - t_n$. Given $U^n \in K_h$, the IMEX approximation computes U^{n+1} from

$$\begin{cases} (U_0^n)^{\gamma-1}\dfrac{U_0^{n+1} - U_0^n}{\Delta t_n} = (A_h U^{n+1})_0 - \dfrac{2}{h_1}(U_0^n)^{-\beta}, \\ (U_i^n)^{\gamma-1}\dfrac{U_i^{n+1} - U_i^n}{\Delta t_n} = (A_h U^{n+1})_i, \qquad 1 \le i \le I. \end{cases} \tag{10}$$

Equivalently, with

$$C^n = \operatorname{diag}\big((U_0^n)^{\gamma-1}, \ldots, (U_I^n)^{\gamma-1}\big), \qquad B(U^n) = \left(-\frac{2}{h_1}(U_0^n)^{-\beta}, 0, \ldots, 0\right)^T,$$

we have

$$(C^n - \Delta t_n A_h)U^{n+1} = C^n U^n + \Delta t_n B(U^n). \tag{11}$$

The time step is chosen before the linear solve:

$$\Delta t_n = \min\left\{\Delta t_{\max},\ \theta_b h_1 (U_0^n)^{\beta+\gamma},\ \theta_q (U_0^n)^{\gamma+2\beta+1}\right\}, \tag{12}$$

where $0 < \theta_b < 1/2$, $\theta_q > 0$, and $\Delta t_{\max} > 0$. The second term bounds the explicit singular boundary decrement and preserves positivity. The third term is based on the rate (6) and refines the time step in the final boundary layer.

Proposition 4.1. *Let $U^n \in K_h$. If Δt_n satisfies* (12) *with $0 < \theta_b < 1/2$, then* (10) *has a unique solution $U^{n+1} \in (0,\infty)^{I+1}$. Moreover, if the solution satisfies*

$$U_0^{n+1} \le U_1^{n+1} \le \cdots \le U_I^{n+1},$$

then $U^{n+1} \in K_h$.

Proof. By Lemma 3.1, $C^n - \Delta t_n A_h$ is a nonsingular M-matrix. Hence it is invertible and its inverse is nonnegative. The right-hand side in (11) is positive in all components except possibly the first. Its first component equals

$$(U_0^n)^\gamma - \frac{2\Delta t_n}{h_1}(U_0^n)^{-\beta}.$$

The restriction $\Delta t_n \le \theta_b h_1 (U_0^n)^{\beta+\gamma}$ gives

$$(U_0^n)^\gamma - \frac{2\Delta t_n}{h_1}(U_0^n)^{-\beta} \ge (1-2\theta_b)(U_0^n)^\gamma > 0.$$

All other components are strictly positive. Multiplication by the nonnegative inverse therefore yields $U^{n+1} > 0$. If the new vector is nondecreasing, then it belongs to K_h by definition. □

5. THE CRANK–NICOLSON DIFFUSION AVERAGE

We next introduce the second time discretization. Only the diffusion term is averaged in time; the singular boundary flux is still evaluated at the known level to keep a linear system at each step.

The Crank–Nicolson variant uses the trapezoidal average of the diffusion term and keeps the singular boundary flux at the known time level. Given $U^n \in K_h$, compute U^{n+1} from

$$\begin{cases} (U_0^n)^{\gamma-1}\dfrac{U_0^{n+1}-U_0^n}{\Delta t_n} = \dfrac{1}{2}(A_h U^{n+1})_0 + \dfrac{1}{2}(A_h U^n)_0 - \dfrac{2}{h_1}(U_0^n)^{-\beta}, \\ (U_i^n)^{\gamma-1}\dfrac{U_i^{n+1}-U_i^n}{\Delta t_n} = \dfrac{1}{2}(A_h U^{n+1})_i + \dfrac{1}{2}(A_h U^n)_i, \qquad 1 \le i \le I. \end{cases} \tag{13}$$

In matrix form,

$$\left(C^n - \frac{\Delta t_n}{2}A_h\right)U^{n+1} = \left(C^n + \frac{\Delta t_n}{2}A_h\right)U^n + \Delta t_n B(U^n). \tag{14}$$

The same boundary positivity restriction is used, but the explicit half-diffusion contribution requires an additional positivity restriction. Define

$$\Lambda_h(U^n) = \max_{0\le i\le I} \frac{|(A_h U^n)_i|}{(U_i^n)^\gamma}. \tag{15}$$

The Crank–Nicolson step is chosen so that

$$\Delta t_n \le \min\left\{\Delta t_{\max},\ \theta_b h_1 (U_0^n)^{\beta+\gamma},\ \theta_c \Lambda_h(U^n)^{-1},\ \theta_q (U_0^n)^{\gamma+2\beta+1}\right\}, \tag{16}$$

where $0 < \theta_b < 1/2$, $0 < \theta_c < 1$, and $\Lambda_h(U^n)^{-1} = +\infty$ if $\Lambda_h(U^n) = 0$.

Proposition 5.1. *Let $U^n \in K_h$. Assume that* (16) *holds and that*

$$2\theta_b + \frac{\theta_c}{2} < 1.$$

Then (13) *has a unique positive solution $U^{n+1} \in (0,\infty)^{I+1}$. If, in addition, the new vector is nondecreasing, then $U^{n+1} \in K_h$.*

Proof. Lemma 3.1, with $\sigma = 1/2$, shows that $C^n - \Delta t_n A_h/2$ is a nonsingular M-matrix with nonnegative inverse. It remains to prove positivity of the right-hand side in (14).

For $1 \le i \le I$, the i-th component is

$$(U_i^n)^\gamma + \frac{\Delta t_n}{2}(A_h U^n)_i.$$

By (15) and (16),

$$\left|\frac{\Delta t_n}{2}(A_h U^n)_i\right| \le \frac{\theta_c}{2}(U_i^n)^\gamma.$$

Thus this component is at least $(1 - \theta_c/2)(U_i^n)^\gamma > 0$. At the active boundary, the right-hand side equals

$$(U_0^n)^\gamma + \frac{\Delta t_n}{2}(A_h U^n)_0 - \frac{2\Delta t_n}{h_1}(U_0^n)^{-\beta}.$$

The explicit diffusion contribution is bounded below by $-\theta_c (U_0^n)^\gamma/2$, and the boundary restriction gives

$$\frac{2\Delta t_n}{h_1}(U_0^n)^{-\beta} \le 2\theta_b (U_0^n)^\gamma.$$

Consequently the first component is bounded below by

$$\left(1 - \frac{\theta_c}{2} - 2\theta_b\right)(U_0^n)^\gamma > 0.$$

Multiplication by the nonnegative inverse yields $U^{n+1} > 0$. The last assertion follows from the definition of K_h. □

Remark 5.1. *In this paper, Crank–Nicolson refers to the trapezoidal treatment of the diffusion term. The singular boundary flux is kept explicit so that each step remains linear and the positivity restriction can be written explicitly. On intervals strictly before quenching this gives first-order consistency for the boundary flux unless a predictor-corrector or trapezoidal regularization of $s^{-\beta}$ is added. Thus the Crank–Nicolson variant is used to test the effect of trapezoidal diffusion averaging, not as a claim of second-order temporal accuracy up to the singular time.*

6. POSITIVITY, COMPARISON AND STABILITY

The qualitative analysis has three steps: inverse positivity of the tridiagonal resolvent, positivity of the solution already obtained in Propositions 4.1 and 5.1, and subcritical stability. The last point is used in the convergence proof.

Proposition 6.1. *Let $C = \mathrm{diag}(c_0, \dots, c_I)$ with $c_i > 0$, let $\sigma \in \{1, 1/2\}$, and let $\Delta t > 0$. If $Y, Z \in \mathbb{R}^{I+1}$ solve*

$$(C - \sigma \Delta t A_h)Y = F, \qquad (C - \sigma \Delta t A_h)Z = G,$$

with $F \le G$ componentwise, then $Y \le Z$ componentwise. Hence the implicit diffusion step used in both schemes is order preserving.

Proof. By Lemma 3.1, $C - \sigma \Delta t A_h$ is a nonsingular M-matrix and its inverse is componentwise nonnegative. Therefore

$$Z - Y = (C - \sigma \Delta t A_h)^{-1}(G - F) \ge 0.$$

□

Remark 6.1. *Proposition 6.1 is the comparison result used below. It avoids an artificial global monotonicity claim for the nonlinear map $U^n \mapsto U^{n+1}$, because its coefficients contain $(U_i^n)^{\gamma-1}$. On every subcritical interval, this nonlinear dependence is handled by Lipschitz stability. The singular boundary source has the monotonicity needed for comparison: if $0 < a \le b$, then $-a^{-\beta} \le -b^{-\beta}$.*

Assumption 6.1. *Whenever boundary localization is invoked, we assume that the computed solution remains in K_h up to the considered stopping level:*

$$0 < U_0^n \le U_1^n \le \cdots \le U_I^n.$$

This assumption is the discrete analogue of Lemma 2.1. Positivity follows from the M-matrix structure. The monotonicity part is a cone-invariance condition that is checked during the computation.

Proposition 6.2. *Let $T < T_q$. Suppose that two numerical solutions U^n and V^n generated by the same scheme, with the same time step Δt_n, remain in a fixed interval*

$$m_T \le U_i^n, V_i^n \le M_T, \qquad 0 < m_T < M_T < \infty,$$

for all $0 \le i \le I$ and all $t_n \le T$. Assume in addition that their discrete diffusion terms are bounded on this interval, namely

$$\|A_h U^n\|_\infty + \|A_h V^n\|_\infty \le K_T, \qquad t_n \le T.$$

Then there exists $C_T > 0$, depending on m_T, M_T and K_T but independent of H, $\Delta t_{\max}$ and n, such that for either the IMEX scheme or the Crank–Nicolson diffusion average,

$$\left\|U^{n+1} - V^{n+1}\right\|_\infty \le (1 + C_T \Delta t_n) \left\|U^n - V^n\right\|_\infty . \tag{17}$$

Proof. We give the proof for the IMEX scheme. The Crank–Nicolson case is identical after replacing A_h by $A_h/2$ in the implicit part and treating the known half-diffusion term with the same subcritical Lipschitz bound.

On $[m_T, M_T]$, the functions $s \mapsto s^{\gamma-1}$ and $s \mapsto s^{-\beta}$ are Lipschitz. Let their Lipschitz constants be L_γ and L_β, and set

$$c_* = \min_{m_T \le s \le M_T} s^{\gamma-1} > 0, \qquad c^* = \max_{m_T \le s \le M_T} s^{\gamma-1}.$$

The first step is to control the one-step increment. From the scheme, the positivity restriction, the subcritical bounds and the assumed bound on the discrete diffusion terms, together with the bounded inverse estimate

$$(C^n - \Delta t_n A_h)^{-1} C^n \mathbf{1} = \mathbf{1},$$

we obtain

$$\left\|U^{n+1} - U^n\right\|_\infty \le C_T \Delta t_n, \qquad \left\|V^{n+1} - V^n\right\|_\infty \le C_T \Delta t_n. \tag{18}$$

The constant depends on the subcritical bounds and on K_T, but not on H or on Δt_n.

Subtract the two IMEX equations and write $C_U^n = \mathrm{diag}((U_i^n)^{\gamma-1})$. Then

$$(C_U^n - \Delta t_n A_h)(U^{n+1} - V^{n+1}) = C_U^n (U^n - V^n) + R^n, \tag{19}$$

where R^n contains the coefficient differences

$$\left((V_i^n)^{\gamma-1} - (U_i^n)^{\gamma-1}\right)(V_i^{n+1} - V_i^n)$$

and the explicit singular boundary difference. Using the Lipschitz bounds and (18),

$$\left\|R^n\right\|_\infty \le C_T \Delta t_n \left\|U^n - V^n\right\|_\infty .$$

The resolvent estimate follows from inverse positivity and

$$(C_U^n - \Delta t_n A_h)\mathbf{1} = C_U^n \mathbf{1}.$$

Indeed, if $|W| \le r\mathbf{1}$, then

$$\left|(C_U^n - \Delta t_n A_h)^{-1} W\right| \le r (C_U^n - \Delta t_n A_h)^{-1} \mathbf{1} \le \frac{r}{c_*} \mathbf{1}.$$

Applying this estimate to (19) gives

$$\left\|U^{n+1} - V^{n+1}\right\|_\infty \le (1 + C_T \Delta t_n) \left\|U^n - V^n\right\|_\infty ,$$

which is (17). □

7. NUMERICAL HITTING TIME AND LOCALIZATION

We now define the numerical event time and prove that the threshold is reached in finite accumulated time under a discrete energy inequality.

The discrete quenching time is detected through a positive threshold. For $\varepsilon > 0$, define

$$n_\varepsilon = \min\{n \geq 0 : U_0^n \leq \varepsilon\}, \qquad T_{h,\Delta t}^\varepsilon = \sum_{k=0}^{n_\varepsilon - 1} \Delta t_k.$$

This threshold is the stopping level used in the computations. It is not a replacement for the singular time. The limit $\varepsilon \downarrow 0$ is taken after the mesh and time-step limits.

For the finite-time statement we use the weighted discrete energy

$$E_h^n = \sum_{i=0}^{I} \omega_i (U_i^n)^\gamma.$$

The hitting-time proof uses the following discrete energy condition. When $\gamma = 1$, the condition follows directly for both schemes by summing (9). For $\gamma \neq 1$, it is a one-step condition to be verified for the nonlinear time discretization.

Assumption 7.1. *There exist $\rho \in [0, 1)$ and $n_* \geq 0$ such that, as long as $U_0^n > \varepsilon$ and $n \geq n_*$,*

$$E_h^{n+1} \leq E_h^n - \gamma(1 - \rho)\Delta t_n (U_0^n)^{-\beta}. \tag{20}$$

Lemma 7.1. *If $\gamma = 1$, then* (20) *holds with $\rho = 0$ for both the IMEX scheme and the Crank–Nicolson diffusion average.*

Proof. For $\gamma = 1$, $E_h^n = \sum_i \omega_i U_i^n$. Multiplying each row of the IMEX scheme by ω_i, summing over i, and using (9), we obtain

$$\frac{E_h^{n+1} - E_h^n}{\Delta t_n} = -(U_0^n)^{-\beta}.$$

This is (20) with $\rho = 0$. For the Crank–Nicolson diffusion average, the weighted sum of $(A_h U^{n+1} + A_h U^n)/2$ is zero by (8), and the explicit singular boundary flux gives the same identity. □

Theorem 7.1. *Assume that the numerical solution remains positive and satisfies Assumption 7.1. Then $n_\varepsilon < \infty$ for every $\varepsilon > 0$. Moreover, the accumulated time before reaching ε is bounded by a constant depending only on E_h^0, β, γ, ρ, and the total weight $\sum_i \omega_i$ in the cone case.*

Proof. Let $W_h = \sum_{i=0}^{I} \omega_i$. If $U^n \in K_h$, then $U_0^n \le U_i^n$ for all i, and hence

$$(U_0^n)^\gamma \le \frac{E_h^n}{W_h}.$$

Thus

$$(U_0^n)^{-\beta} \ge W_h^{\beta/\gamma} (E_h^n)^{-\beta/\gamma}.$$

Without the cone assumption, the same argument holds with the weaker constant $\omega_0^{\beta/\gamma}$. Assumption 7.1 gives

$$E_h^{n+1} \le E_h^n - c_0 \Delta t_n (E_h^n)^{-\beta/\gamma}, \qquad c_0 = \gamma(1-\rho) W_h^{\beta/\gamma} > 0.$$

Since E_h^n is decreasing, the elementary inequality for $p = 1 + \beta/\gamma$ yields

$$(E_h^{n+1})^p \le (E_h^n)^p - p c_0 \Delta t_n.$$

After summation from n_* to $N-1$,

$$(E_h^N)^p \le (E_h^{n_*})^p - p c_0 \sum_{n=n_*}^{N-1} \Delta t_n.$$

The right-hand side becomes negative if the accumulated time is too large. Hence the computation must reach the threshold $U_0^n \le \varepsilon$ before that happens. □

Proposition 7.1. *Assume that $U^0 \in K_h$ and that Assumption 6.1 holds for $0 \le n < n_\varepsilon$. Then the numerical hitting is localized at the active boundary:*

$$U_0^n = \min_{0 \le i \le I} U_i^n, \qquad 0 \le n < n_\varepsilon.$$

Consequently, $T_{h,\Delta t}^\varepsilon$ is detected by the scalar sequence U_0^n.

Proof. The identity follows from $U^n \in K_h$. The proposition separates positivity, which is proved by the M-matrix argument, from the cone condition used to identify the active boundary as the hitting point. □

8. CONVERGENCE BEFORE QUENCHING AND CONVERGENCE OF HITTING TIMES

The convergence analysis is restricted to time intervals separated from the quenching time. On such intervals the exact solution is uniformly positive and the singular boundary flux is locally Lipschitz.

The convergence proof keeps the actual consistency defect. On nonuniform grids, this keeps the boundary and interior truncation errors distinct. Let

$$H^* = \max_{1\le i\le I-1} |h_{i+1} - h_i|, \qquad H = \max_{1\le i\le I} h_i.$$

For the exact solution, set

$$u_h(t_n) = (u(x_0, t_n), \dots, u(x_I, t_n))^T, \qquad e^n = u_h(t_n) - U^n.$$

Let $R_h(T)$ be the consistency defect of the complete nonuniform operator, including the boundary row, obtained by inserting exact grid values into the corresponding time-discrete scheme and taking the maximum over $0 \le t_n \le T$ and $0 \le i \le I$.

For a smooth solution on an interior nonuniform grid, the standard expansion gives

$$\delta_h^2 u(x_i, t) = u_{xx}(x_i, t) + \frac{h_{i+1} - h_i}{3} u_{xxx}(x_i, t) + O(H^2), \qquad 1 \le i \le I - 1.$$

Thus the interior part of the defect is $O(H^2 + H^*)$. The boundary contribution is included in $R_h(T)$. If a second-order boundary-corrected Neumann row is used, or if the compatibility conditions remove the first boundary remainder, then $R_h(T) \le C_T(H^2 + H^*)$. Under Assumption 3.1, this becomes $R_h(T) \le C_T H^2$ for the interior part and for any boundary row with the same order. With the energy-balanced boundary row retained here, the theorem below remains valid with the actual boundary consistency defect.

Theorem 8.1. *Let $T < T_q$. Assume that*

$$u \in C^{4,2}([0,1] \times [0,T]), \qquad \min_{(x,t)\in[0,1]\times[0,T]} u(x,t) = \rho_T > 0,$$

and that the numerical solution remains in a compact subcritical interval $[\rho_T/2, M_T]$ for all $t_n \le T$. Let $\Phi_h = U^0$. Then the IMEX approximation satisfies

$$\max_{0\le t_n\le T} \|U^n - u_h(t_n)\|_\infty \le C_T \left(\|\Phi_h - u_h(0)\|_\infty + R_h(T) + \Delta t_{\max} \right). \tag{21}$$

Under second-order boundary consistency,

$$\max_{0\le t_n\le T} \|U^n - u_h(t_n)\|_\infty \le C_T \left(\|\Phi_h - u_h(0)\|_\infty + H^2 + H^* + \Delta t_{\max} \right). \tag{22}$$

The Crank–Nicolson diffusion average satisfies the same estimate. If the boundary flux is evaluated by a second-order predictor-corrector trapezoidal rule on $[0,T]$, then the temporal contribution for the Crank–Nicolson variant becomes $O(\Delta t_{\max}^2)$ on subcritical intervals.

Proof. We prove the IMEX estimate. Since $T < T_q$, the exact values satisfy $u_i^n \geq \rho_T$. By the subcritical hypothesis, the numerical values lie in $[\rho_T/2, M_T]$. On this interval the functions $s \mapsto s^{\gamma-1}$ and $s \mapsto s^{-\beta}$ are Lipschitz.

Insert $u_h(t_n)$ into the IMEX scheme. By the definition of $R_h(T)$, the exact grid values satisfy the perturbed discrete system

$$(u_i^n)^{\gamma-1}\frac{u_i^{n+1}-u_i^n}{\Delta t_n} - (A_h u^{n+1})_i = \Theta_i^n, \qquad 1 \leq i \leq I,$$
$$(u_0^n)^{\gamma-1}\frac{u_0^{n+1}-u_0^n}{\Delta t_n} - (A_h u^{n+1})_0 + \frac{2}{h_1}(u_0^n)^{-\beta} = \Theta_0^n,$$

with

$$\|\Theta^n\|_\infty \leq C_T(R_h(T) + \Delta t_n).$$

Subtracting the numerical scheme gives

$$(C_u^n - \Delta t_n A_h)e^{n+1} = C_u^n e^n + \Delta t_n Q^n + \Delta t_n \Theta^n,$$

where $C_u^n = \mathrm{diag}((u_i^n)^{\gamma-1})$ and Q^n contains only nonlinear coefficient differences. The mean-value theorem on $[\rho_T/2, M_T]$ gives

$$\|Q^n\|_\infty \leq C_T \|e^n\|_\infty .$$

Let

$$B_h = \|\Phi_h - u_h(0)\|_\infty + R_h(T) + \Delta t_{\max}, \qquad V_i^n = Ke^{\Lambda t_n} B_h,$$

where $K \geq 1$ and $\Lambda > 0$ will be fixed. Since V^n is spatially constant, $A_h V^{n+1} = 0$. Moreover,

$$(C_u^n - \Delta t_n A_h)V^{n+1} - C_u^n V^n = C_u^n(V^{n+1} - V^n) \geq c_* K\Lambda e^{\Lambda t_n}\Delta t_n B_h,$$

where $c_* = \min_{s\in[\rho_T/2, M_T]} s^{\gamma-1} > 0$, for sufficiently small $\Delta t_{\max}$. Choosing K and Λ sufficiently large gives

$$(C_u^n - \Delta t_n A_h)V^{n+1} - C_u^n V^n \geq \Delta t_n(|Q^n| + |\Theta^n|)$$

componentwise. Since $V^0 \geq |e^0|$, Proposition 6.1 applied to $V^n - e^n$ and $V^n + e^n$ yields

$$|e^n| \leq V^n, \qquad 0 \leq t_n \leq T.$$

Therefore

$$\|e^n\|_\infty \leq Ke^{\Lambda T} B_h, \qquad 0 \leq t_n \leq T,$$

which proves (21). Estimate (22) follows from the second-order consistency statement. The Crank–Nicolson proof is the same, with the explicit half-diffusion term included in the perturbation. The order of the temporal defect is first order for the frozen singular flux used in (13); it becomes second order if this boundary flux is evaluated by a trapezoidal predictor-corrector formula. □

Remark 8.1. *The term H^* is standard for nonuniform central differences. Even when H is small, abrupt variation of neighboring steps enters the truncation error through $h_{i+1} - h_i$. For smooth stretching functions such as* (7)*, $H^* = O(H^2)$, and the usual second-order interior estimate is recovered away from boundary defects.*

Theorem 8.2. *Let $\varepsilon > 0$ be a regular level for $d(t) = u(0,t)$. Assume that $d(t) = \varepsilon$ has a unique solution $T^\varepsilon < T_q$ and that*

$$|d'(T^\varepsilon)| \geq \mu_\varepsilon > 0.$$

Then, for either scheme,

$$|T^\varepsilon_{h,\Delta t} - T^\varepsilon| \leq C_\varepsilon \left(\|\Phi_h - u_h(0)\|_\infty + R_h(T^\varepsilon + \rho) + \Delta t_{\max} \right), \tag{23}$$

for some $\rho > 0$ such that $[T^\varepsilon - \rho, T^\varepsilon + \rho] \subset (0, T_q)$, provided H and $\Delta t_{\max}$ are sufficiently small. Under second-order boundary consistency,

$$|T^\varepsilon_{h,\Delta t} - T^\varepsilon| \leq C_\varepsilon \left(\|\Phi_h - u_h(0)\|_\infty + H^2 + H^* + \Delta t_{\max} \right).$$

Consequently,

$$\lim_{\varepsilon \downarrow 0} \lim_{\Delta t_{\max} \downarrow 0} \lim_{H \downarrow 0} T^\varepsilon_{h,\Delta t} = T_q,$$

whenever the corresponding consistency defect tends to zero.

Proof. Choose $\rho > 0$ such that $[T^\varepsilon - \rho, T^\varepsilon + \rho] \subset (0, T_q)$. Theorem 8.1 gives

$$\max_{t_n \leq T^\varepsilon + \rho} |U_0^n - u(0, t_n)| \leq C \left(\|\Phi_h - u_h(0)\|_\infty + R_h(T^\varepsilon + \rho) + \Delta t_{\max} \right).$$

Because $|d'(T^\varepsilon)| \geq \mu_\varepsilon$, the inverse crossing map is Lipschitz near T^ε. After reducing ρ if necessary,

$$|t - T^\varepsilon| \leq \frac{2}{\mu_\varepsilon} |d(t) - \varepsilon|, \qquad |t - T^\varepsilon| \leq \rho.$$

By definition, n_ε is the first index for which $U_0^n \leq \varepsilon$, while $U_0^{n_\varepsilon - 1} > \varepsilon$ when $n_\varepsilon > 0$. Applying the uniform boundary error estimate at these two neighboring levels and adding one time step gives (23). Finally, $T^\varepsilon \uparrow T_q$ as $\varepsilon \downarrow 0$, because $u(0,t) > 0$ for $t < T_q$ and $u(0,t) \to 0$ as $t \to T_q^-$. □

9. NUMERICAL EXPERIMENTS

We now report the numerical tests used to check the properties proved above. All simulations use either the IMEX scheme (10)–(12) or the Crank–Nicolson diffusion-average scheme (13)–(16). In both schemes the singular boundary flux is evaluated at the previous time level, and the time step is chosen before each linear solve.

9.1. IMEX and Crank–Nicolson comparison

For the tests we set

$$\beta = 1, \qquad \gamma = 1,$$

and use the compatible initial datum

$$u_0(x) = a\cos(1-x), \qquad a = \frac{1}{\sqrt{\sin(1)\cos(1)}}.$$

Then $u_0'(0) = u_0(0)^{-1}$, $u_0'(1) = 0$, and $u_0' \geq 0$ on $[0,1]$. Unless otherwise stated, the nonuniform grid is (7) with $\alpha = 2$. The stopping level for Tables 1 and 2 is $\varepsilon = 10^{-3}$, and $\Delta t_{\max} = 10^{-4}$. The adaptive parameter $\theta_b = 0.25$ is used in all tests, and the same fixed value of θ_q is kept throughout each refinement sequence. For the Crank–Nicolson diffusion average, the extra restriction (16) is imposed with $\theta_c = 0.5$.

The observed spatial indicator is

$$s_I = \log_2\left(\frac{T_{I/4} - T_{I/2}}{T_{I/2} - T_I}\right),$$

whenever three consecutive values are available and the differences have the same sign.

Table 1 reports the computed hitting times for the two schemes. Both sequences stabilize under refinement. On the same grids, the Crank–Nicolson diffusion average reaches the threshold slightly earlier than the IMEX scheme. The observed indicators remain near two over most refinements; the last IMEX value deviates because the final refinements are already close to the threshold and time-step tolerance scale.

Table 1: IMEX and Crank–Nicolson hitting times on the nonuniform grid $\alpha = 2$, with $\varepsilon = 10^{-3}$ and $\Delta t_{\max} = 10^{-4}$.

I	$h_{\min}$	$T^{\varepsilon}_{h,\Delta t}$ IMEX	s IMEX	$T^{\varepsilon}_{h,\Delta t}$ CN	s CN
16	2.0840×10^{-2}	0.16453336	–	0.16439480	–
32	1.0095×10^{-2}	0.16405507	–	0.16390770	–
64	4.9700×10^{-3}	0.16392351	1.86	0.16377273	1.85
128	2.4650×10^{-3}	0.16388781	1.88	0.16373565	1.86
256	1.2270×10^{-3}	0.16387806	1.87	0.16372559	1.88
512	6.1260×10^{-4}	0.16387516	1.75	0.16372287	1.89

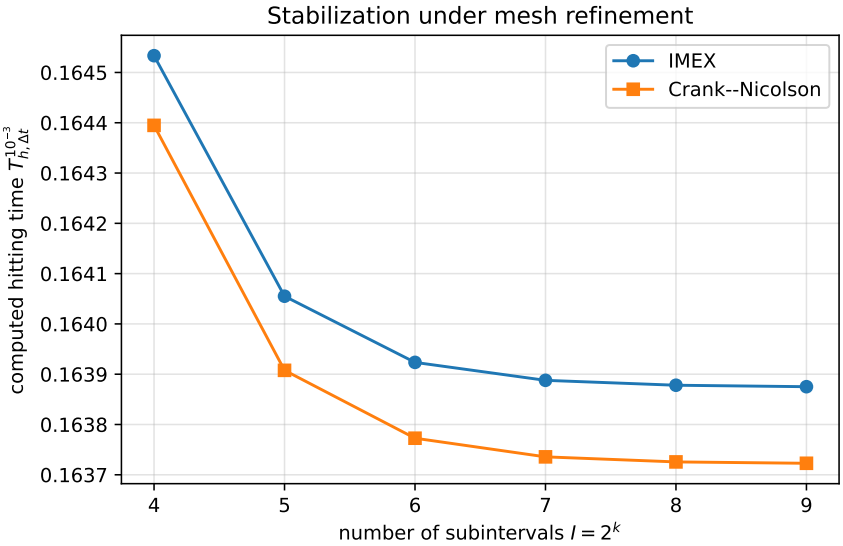

Figure 1: Computed hitting times for the IMEX and Crank–Nicolson diffusion-average schemes. Both sequences stabilize as I increases.

9.2. Effect of the nonuniform grid

Table 2 compares a uniform grid with the exponential nonuniform grid. For small values of I, the nonuniform grid gives a hitting time closer to the refined IMEX value because it places more nodes near the active boundary. As I increases, the uniform and nonuniform values approach each other because both grids resolve the boundary layer.

Table 2: Uniform and nonuniform grid comparison for the IMEX scheme with $\varepsilon = 10^{-3}$.

I	T_{unif}	T_{nonunif}	difference
16	0.16628245	0.16453336	1.7491×10^{-3}
32	0.16423055	0.16405507	1.7548×10^{-4}
64	0.16397080	0.16392351	4.7290×10^{-5}
128	0.16390260	0.16388781	1.4790×10^{-5}
256	0.16388420	0.16387806	6.1400×10^{-6}
512	0.16387780	0.16387516	2.6400×10^{-6}

Figure 2 displays the mesh distribution and the active boundary value. The left panel displays the concentration of nodes near x=0 The right panel indicates that $U_0(t)$ remains

positive until the stopping level and then decreases rapidly near the hitting time. This decay justifies the adaptive terms in (12) and (16).

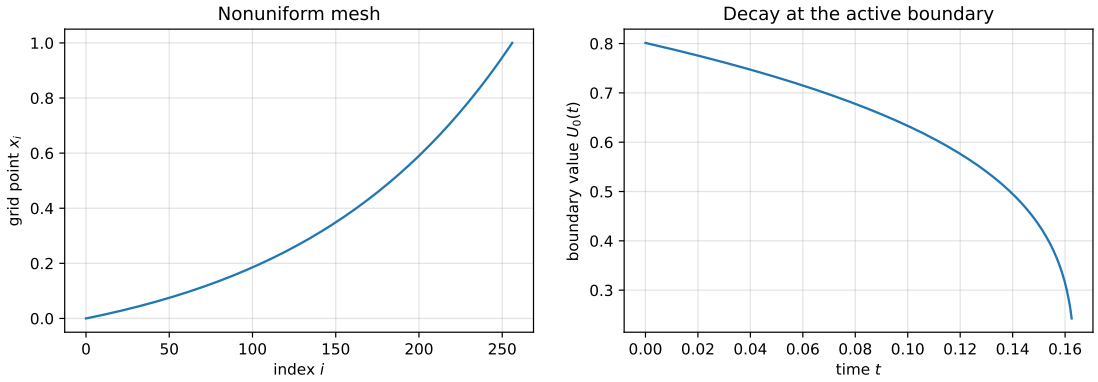

(a) Nonuniform mesh. **(b)** Active boundary value.

Figure 2: Nonuniform mesh and active boundary value. The boundary value remains positive before the stopping level and decreases as the hitting time is approached.

9.3. Influence of the stopping threshold

Table 3 reports the influence of the stopping threshold. The first line is not a computation at the level $\varepsilon = 0$; it is a reference computed with $\varepsilon_{\mathrm{ref}} = 10^{-5}$. For $\varepsilon = 10^{-3}$ and $\varepsilon = 10^{-4}$, the variations from the reference are 3.00×10^{-7} and 4.00×10^{-8}, respectively.

Table 3: Influence of the stopping threshold on the computed IMEX boundary hitting time for $I = 256$.

threshold ε	computed time	variation from reference
$\varepsilon_{\mathrm{ref}} = 10^{-5}$	0.16387836	0
10^{-1}	0.16382673	5.163×10^{-5}
10^{-2}	0.16387812	2.40×10^{-7}
10^{-3}	0.16387806	3.00×10^{-7}
10^{-4}	0.16387832	4.00×10^{-8}

9.4. Profiles, rate and space-time representation

Figure 3 contains the profile and rate diagnostics. The profile panel indicates that the minimum remains at the active boundary and that the interior stays positive at

the displayed times. The rate panel compares the computed boundary value with the reference slope

$$\frac{1}{\gamma + 2\beta + 1} = \frac{1}{4},$$

which is the exponent predicted by Proposition 2.2. Near the computed hitting time, the numerical curve is parallel to the reference line. Away from quenching, the asymptotic law does not determine the profile.

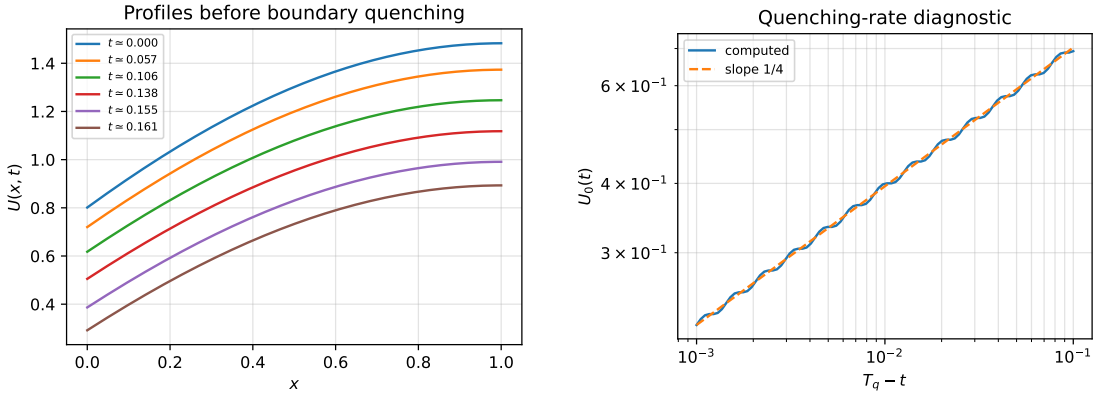

(a) Profiles before boundary quenching. **(b)** Quenching-rate diagnostic.

Figure 3: Boundary localization and rate verification. The left panel indicates that the smallest values stay at $x = 0$. The right panel agrees with the theoretical exponent.

Figure 4 gives a space-time representation of the computed solution. The plot localizes the decay at the active boundary, while the interior remains positive on the displayed time interval.

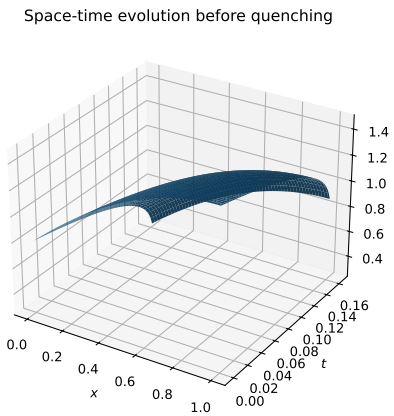

Figure 4: Space-time evolution before boundary quenching. The decay is concentrated near the active boundary $x = 0$.

The numerical tests support the analysis. The schemes preserve positivity under the stated adaptive restrictions, the hitting times stabilize under refinement, the nonuniform grid reduces the coarse-mesh error near the singular boundary, and the boundary rate agrees with the theoretical exponent. The Crank–Nicolson diffusion average reduces diffusion error but requires a stronger positivity check than the IMEX method.

10. FINAL REMARKS AND PERSPECTIVES

We developed a nonuniform-grid time-discrete analysis for the Christov–Deng type boundary-quenching problem. The proof separates the spatial concentration near the active boundary, the singular boundary flux, and the time integration. The IMEX method preserves positivity through an M-matrix solve. The Crank–Nicolson diffusion average uses a trapezoidal treatment of diffusion but must be accompanied by an explicit positivity restriction because the singular boundary flux is frozen in the present linear form.

The first continuation is to add a second-order predictor-corrector treatment of the singular boundary flux in the Crank–Nicolson variant, so that the temporal consistency improves on subcritical intervals. The second extension is to replace the fixed stretched grid by an adaptive moving grid following the boundary layer. The third direction is to transfer the same IMEX and Crank–Nicolson strategy to interior localized singularities, where the mesh must concentrate around an unknown or prescribed quenching point. A further continuation is to combine this analysis with finite-volume or multiscale discretizations on general grids, especially for heterogeneous diffusion coefficients.

REFERENCES

[1] A. Acker and W. Walter, The quenching problem for nonlinear parabolic differential equations, in *Ordinary and Partial Differential Equations*, Lecture Notes in Mathematics 564, Springer, Berlin, 1976, pp. 1–12.

[2] A. Babucke and M. J. Kloker, Accuracy analysis of finite-difference methods on non-uniform grids, Institut für Aerodynamik und Gasdynamik, Universität Stuttgart, Report IB 09-01, 2009.

[3] C. I. Christov and K. Deng, Numerical investigation of quenching for a nonlinear diffusion equation with a singular Neumann boundary condition, *Numerical Methods for Partial Differential Equations* 18 (2002), 429–440.

[4] K. Deng and H. A. Levine, On the blow-up of u_t at quenching, *Proceedings of the American Mathematical Society* 106 (1989), 1049–1056.

[5] K. Deng and M. Xu, Quenching for a nonlinear diffusion equation with a singular boundary condition, *Zeitschrift für Angewandte Mathematik und Physik* 50 (1999),

574–584.

[6] M. Fila, B. Kawohl and H. A. Levine, Quenching for quasilinear equations, *Communications in Partial Differential Equations* 17 (1992), 593–614.

[7] M. Fila and H. A. Levine, Quenching on the boundary, *Nonlinear Analysis: Theory, Methods and Applications* 21 (1993), 795–802.

[8] A. Friedman, *Partial Differential Equations of Parabolic Type*, Prentice-Hall, Englewood Cliffs, NJ, 1964.

[9] B. S. Jovanović and P. P. Matus, Finite difference schemes on nonuniform meshes for parabolic problems with generalized solutions, *Publications de l'Institut Mathématique* 67(81) (2000), 145–158.

[10] B. S. Jovanović, Finite difference schemes for partial differential equations with weak solutions and irregular coefficients, *Computational Methods in Applied Mathematics* 4 (2004), 48–65.

[11] I. P. Jones and C. P. Thompson, A note on the use of nonuniform grids in finite difference calculations, A.E.R.E. Harwell Report, 1980.

[12] H. Kawarada, On solutions of initial-boundary value problems for $u_t = u_{xx} + 1/(1-u)$, *Publications of the Research Institute for Mathematical Sciences* 10 (1975), 729–736.

[13] O. A. Ladyzhenskaya, V. A. Solonnikov and N. N. Ural'tseva, *Linear and Quasilinear Equations of Parabolic Type*, Translations of Mathematical Monographs 23, American Mathematical Society, Providence, RI, 1968.

[14] R. D. Lazarov, V. L. Makarov and A. A. Samarskii, Application of exact difference schemes to the construction and study of difference schemes for generalized solutions, *Mathematics of the USSR-Sbornik* 45 (1983), 461–471.

[15] H. A. Levine, The quenching of solutions of linear parabolic and hyperbolic equations with nonlinear boundary conditions, *SIAM Journal on Mathematical Analysis* 14 (1983), 1139–1153.

[16] H. A. Levine, The phenomenon of quenching: a survey, in *Trends in the Theory and Practice of Nonlinear Analysis*, North-Holland, Amsterdam, 1985, pp. 275–286.

[17] K. W. Liang, P. Lin, M. T. Ong and R. C. E. Tan, A splitting moving mesh method for reaction-diffusion equations of quenching type, *Journal of Computational Physics* 215 (2006), 757–777.

[18] K. W. Liang, P. Lin and R. C. E. Tan, Numerical solution of quenching problems using mesh-dependent variable temporal steps, *Applied Numerical Mathematics* 57 (2007), 791–800.

[19] G. M. Lieberman, *Second Order Parabolic Differential Equations*, World Scientific, River Edge, NJ, 1996.

[20] C. V. Pao, *Nonlinear Parabolic and Elliptic Equations*, Plenum Press, New York, 1992.

[21] M. H. Protter and H. F. Weinberger, *Maximum Principles in Differential Equations*, corrected reprint of the 1967 original, Springer, New York, 1984.

[22] A. A. Samarskii, *The Theory of Difference Schemes*, Marcel Dekker, New York, 2001.

[23] A. E. P. Veldman and K. Rinzema, Playing with nonuniform grids, *Journal of Engineering Mathematics* 26 (1992), 119–130.

[24] H. Wang, S. B. Pope and D. A. Caughey, Central-difference schemes on non-uniform grids and their applications in large-eddy simulations of turbulent jets and jet flames, preprint, 2011.